A Heme Propionate Staples the Structure of Cytochrome *c* for Methionine Ligation to the Heme Iron

Yunling Deng[‡], Madeline L. Weaver[§], Kevin R. Hoke[§], and Ekaterina V. Pletneva*[,‡]

[‡]Department of Chemistry, Dartmouth College, Hanover, NH 03755, and [§]Department of Chemistry and Biochemistry, Berry College, Mount Berry, GA 30149

*Corresponding author: ekaterina.pletneva@dartmouth.edu, Tel. 1-603-646-0933, Fax: 1-603-646-3946

Supporting Information

Scheme S1

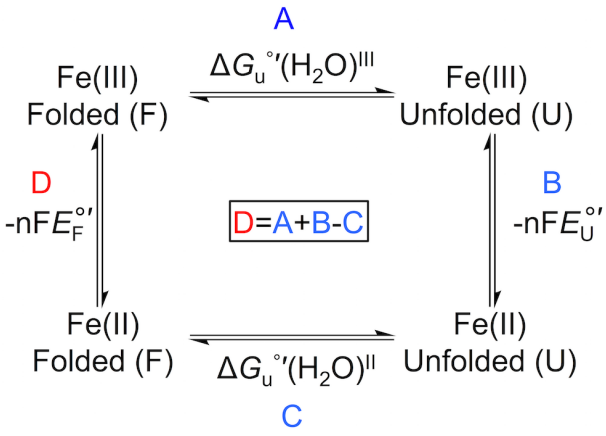

Scheme S2

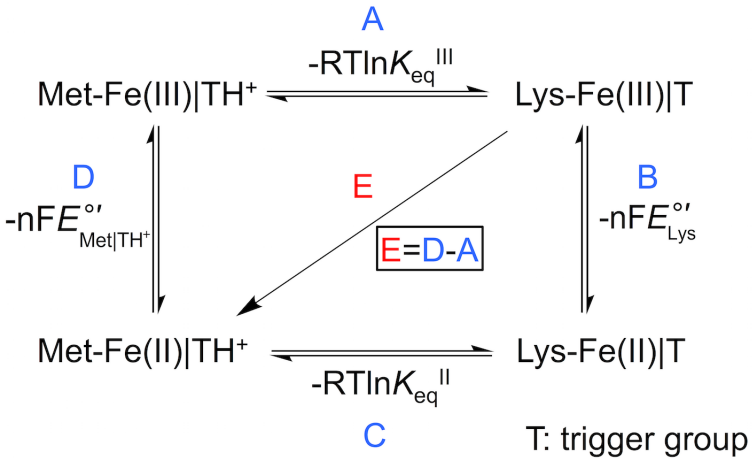

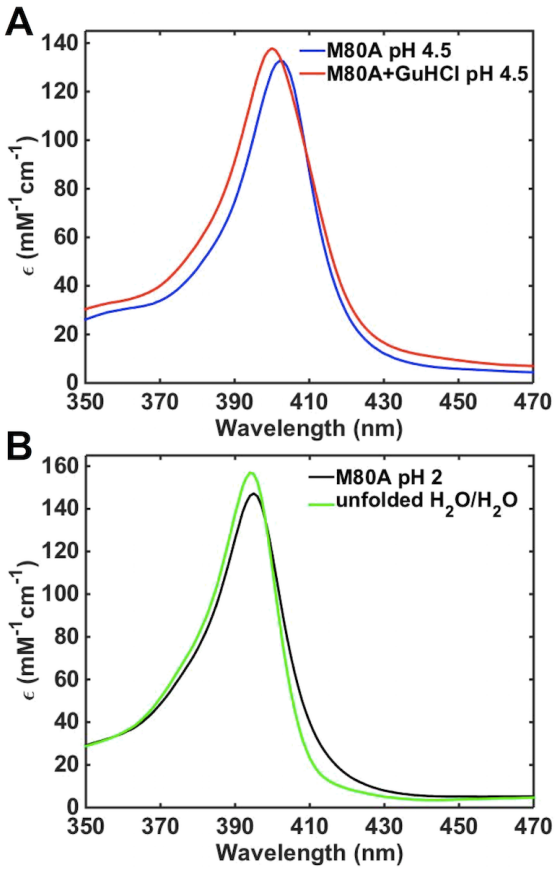

Figure S1. (A) Electronic absorption spectra of ferric M80A yeast *iso*-1 cyt *c*. The spectrum of ferric M80A at pH 4.5 (blue) represents that of ferric H_2O/His folded species. The spectrum of ferric M80A in 3 M GuHCl at pH 4.5 (red) represents that of ferric H_2O/His unfolded species. (B) The spectrum of ferric M80A at pH 2 (black) and the spectrum of ferric H_2O/H_2O unfolded species (green) calculated based on the prior finding that M80A at pH 2 is composed of 75% H_2O/H_2O unfolded and 25% H_2O/His unfolded species.[1] The spectrum of ferric H_2O/H_2O unfolded species was employed as a reference spectrum for Component 1 in the four-component SVD analyses of the pH-dependent spectral series for T49V/K79G and T78V/K79G.

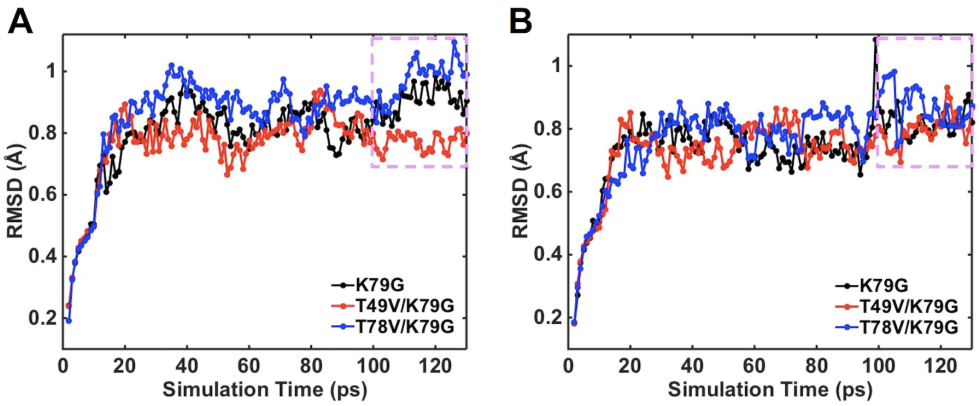

Figure S2. RMSDs of the backbone C_α atoms for each snapshot relative to those from the initial structure in MD simulations of (A) ferric and (B) ferrous Met80-ligated K79G (black), T49V/K79G (red), and T78V/K79G (blue). The purple dash-line rectangles show RMSDs for the last thirty snapshots used for the structural analyses in Tables S2 and S3.

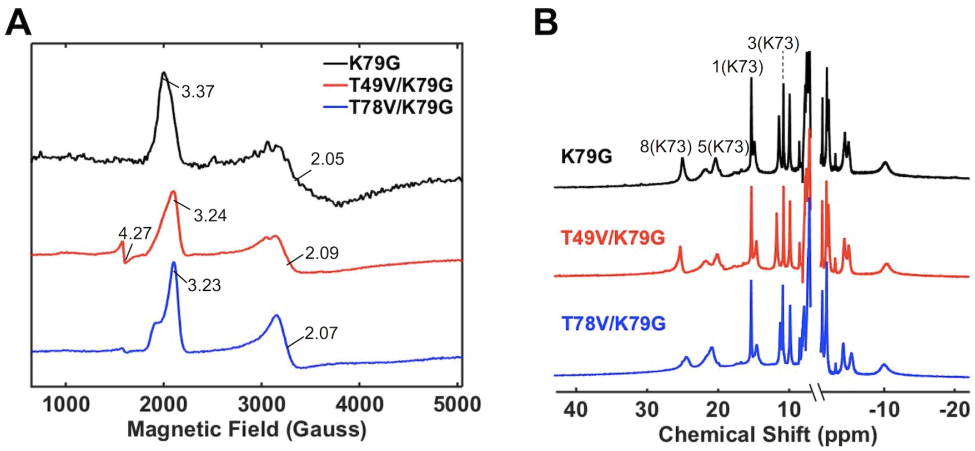

Figure S3. (A) EPR spectra at 10 K and pH 10.5 and (B) ^{1}H NMR spectra at 25 °C and pD 10.5 for ferric K79G (black), T49V/K79G (red), and T78V/K79G (blue).

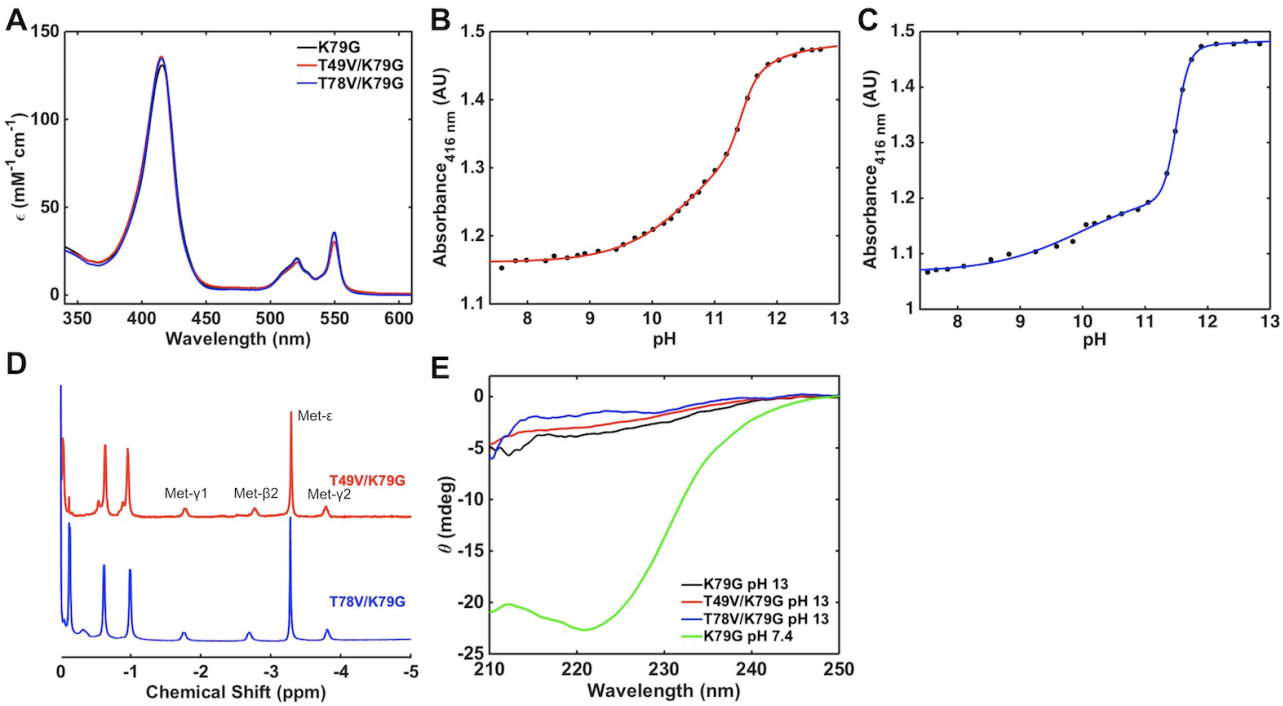

Figure S4. (A) Comparison of electronic absorption spectra of ferrous K79G (black), T49V/K79G (red) and T78V/K79G (blue) at pH 7.4. (B, C) Changes in absorbance at 416 nm during pH titration of ferrous T49V/K79G (B) and T78V/K79G (C) from pH 7.4 to 13. Fits (solid lines) to eq 2 yielded the two pK_a values in Table 2. (D) ^{1}H NMR spectra of ferrous T49V/K79G at pH 11.1 and ferrous T78V/K79G at pH 10.7 at 25 °C. Peak labeling is the same as in Figure 3. (E) Far-UV CD spectra of ferrous K79G (black), T49V/K79G (red), and T78V/K79G (blue) at pH 13 comparing to that of ferrous K79G at pH 7.4 (green).

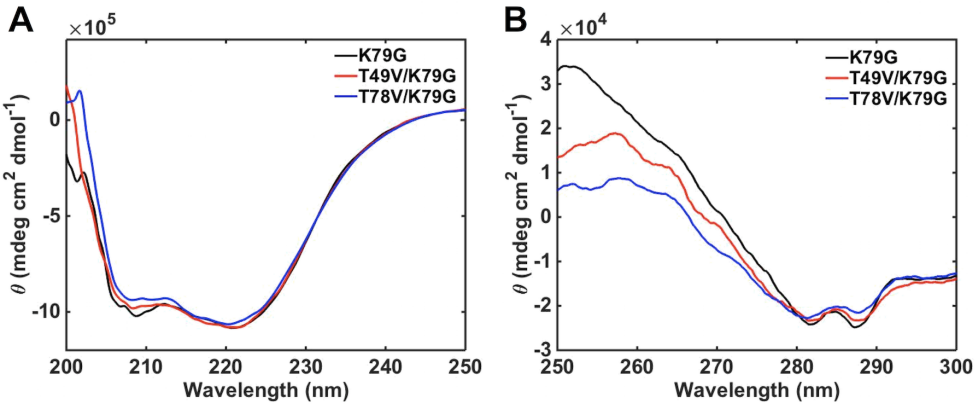

Figure S5. (A) Far- and (B) near-UV CD spectra of ferrous K79G (black), T49V/K79G (red), and T78V/K79G (blue) in a 100 mM sodium phosphate buffer at pH 7.4 and 22 ± 2 °C.

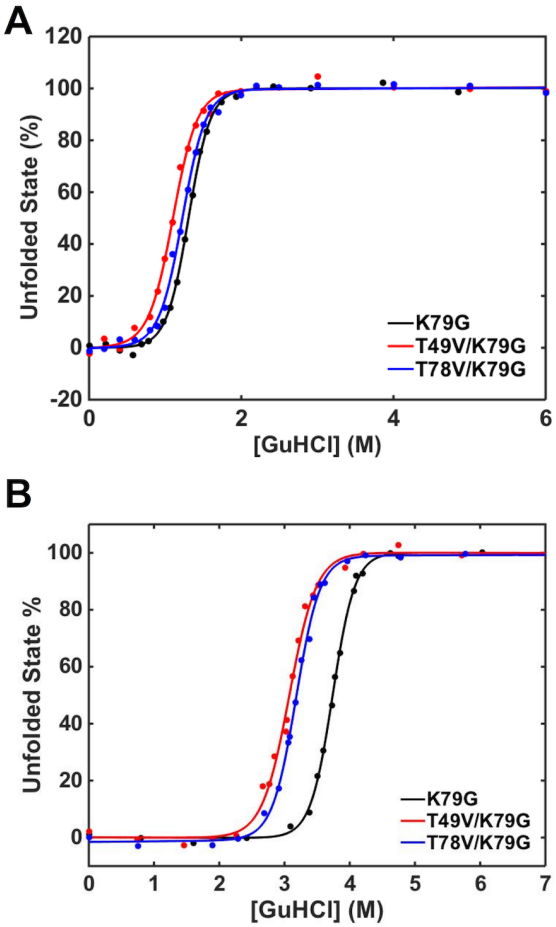

Figure S6. GuHCl titration data for (A) ferric and (B) ferrous K79G (black), T49V/K79G (red), and T78V/K79G (blue) showing normalized changes in the percentage of the unfolded state from CD ellipticity at 222 nm at pH 7.4.

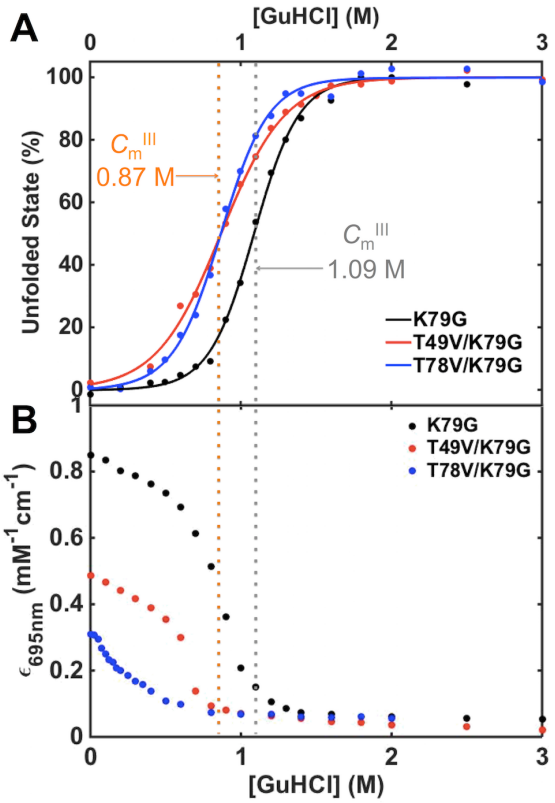

Figure S7. GuHCl titration data for ferric K79G (black), T49V/K79G (red), and T78V/K79G (blue) at pH 4.5. (A) Normalized changes in the percentage of unfolded state from CD ellipticity at 222 nm. (B) Changes in the extinction coefficient at 695 nm from UV-visible spectra. Dashed lines display C_m^{III} values for K79G (gray) and for T49V/K79G and T78V/K79G (orange) from measurements of CD ellipticity at 222 nm.

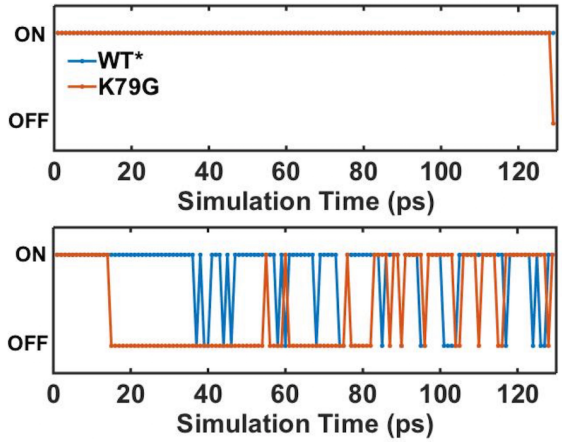

Figure S8. Analyses of hydrogen-bonding interactions in structural models of Met-ligated ferric WT* (blue) and K79G (red). "ON" and "OFF" labels represent the presence and absence of a hydrogen-bonding contact from the side chain oxygen of Thr49 (top) or Thr78 (bottom) to an oxygen atom of HP6.

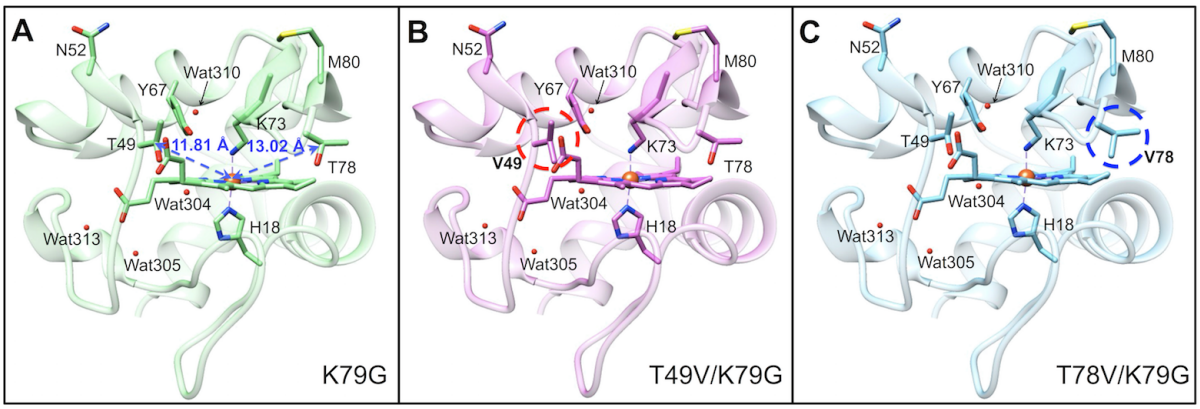

Figure S9. Structural models of Lys73-ligated (A) K79G, (B) T49V/K79G, and (C) T78V/K79G. Water molecules are represented by red spheres and the ferric heme iron is represented by an orange sphere. All variants contain K72A/C102S background mutations. In the absence of force-field parameters for Lys-ligated hemes, these structural models were constructed based on the crystal structure for the Lys-ligated T78C/K79G variant (PDB: 4Q5P).[2] Distances between the C_β atom of residue 49 (or residue 78) and the heme iron are indicated in the model of K79G.

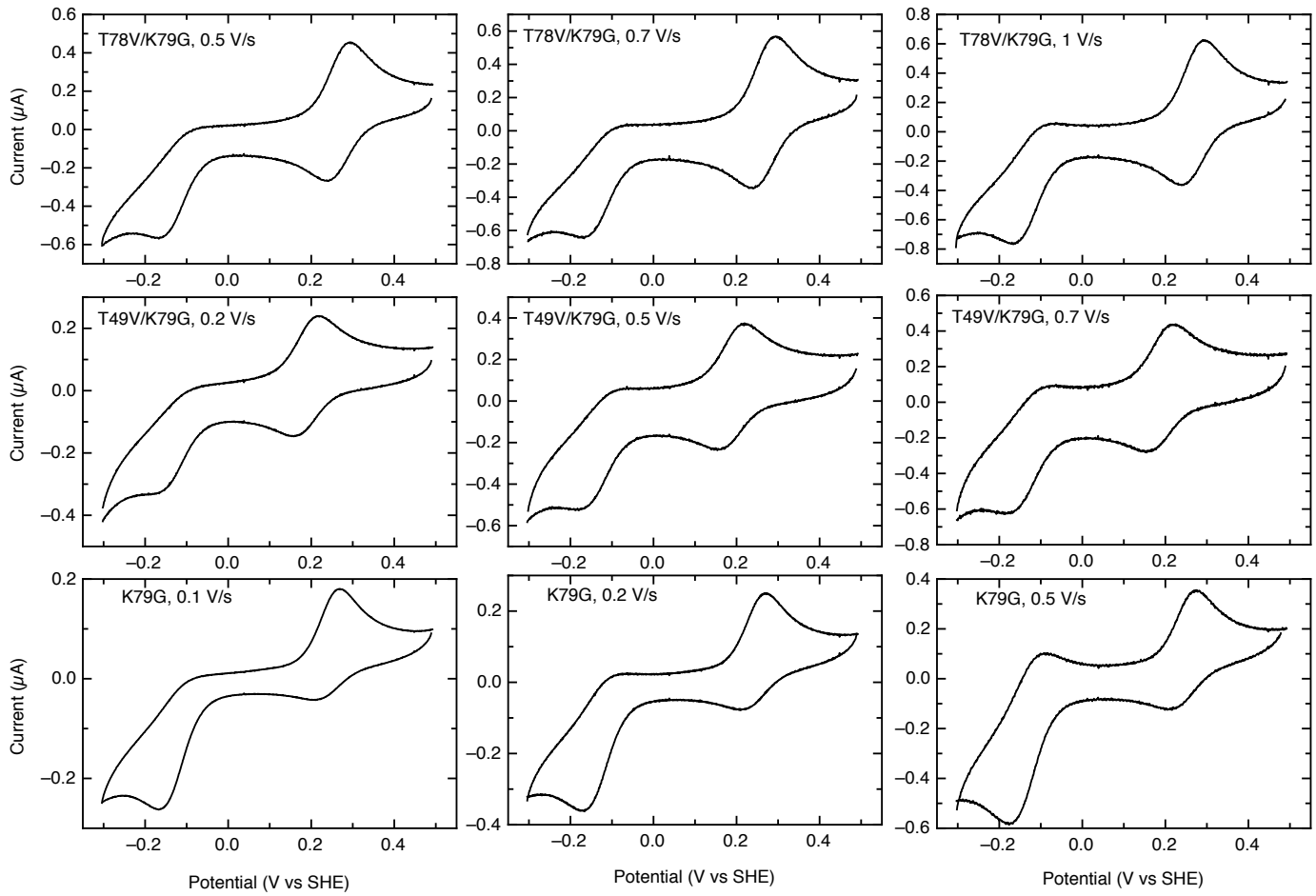

Figure S10. Cyclic voltammograms at varying scan rates (as labeled in V/s) for T78V/K79G (100 μM) and T49V/K79G (90 μM) at pH 7.4, and K79G (110 μM) at pH 10. Cyclic voltammograms shown correspond to the second of two full cycles. A background current corresponding to a capacitance of 0.5 to 0.6 microfarads multiplied by the scan rate was subtracted for each. Each row demonstrates the onset of reversibility at low potential for a different variant. Voltammograms along diagonals from upper left to lower right compare different variants at the same scan rate.

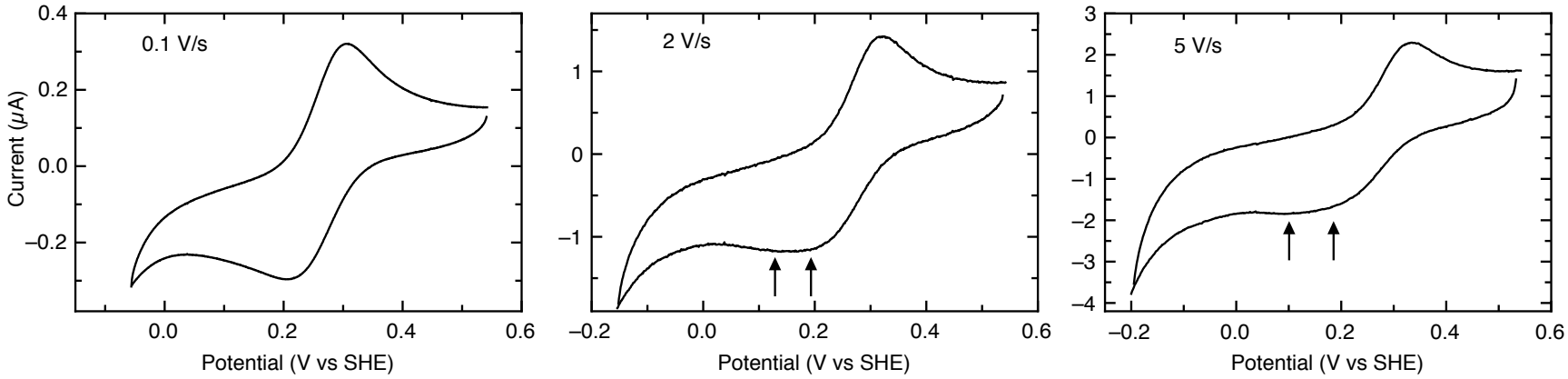

Figure S11. Cyclic voltammograms at a series of scan rates (as labeled) for T78V/K79G at pH 4.5 (0.1 M sodium acetate). Cyclic voltammograms shown correspond to the second of two full cycles. A background current corresponding to a capacitance of 0.5 microfarads multiplied by the scan rate was subtracted in each direction. Arrows note approximate positions of adjacent peaks for two reduction processes in the cyclic voltammograms.

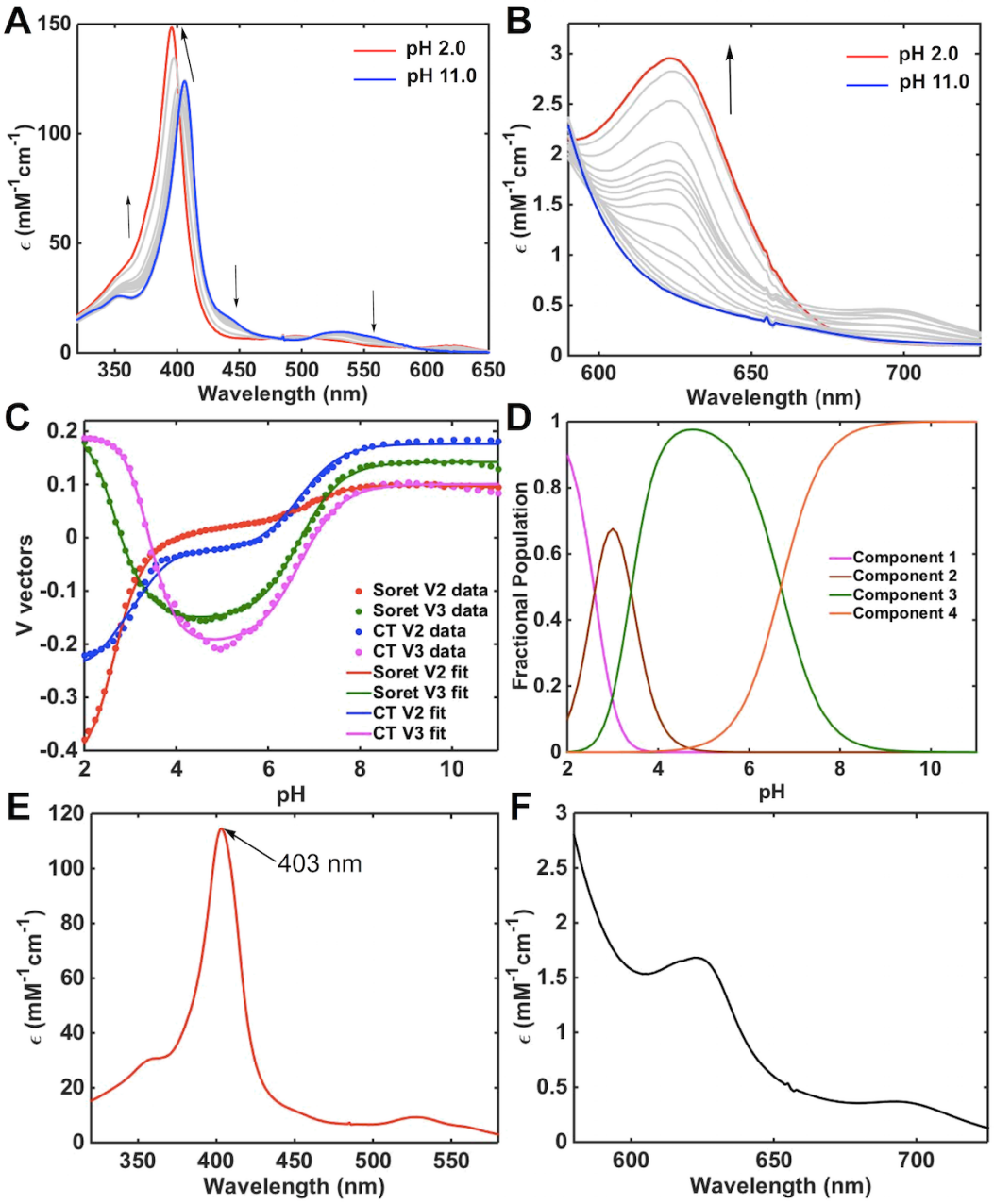

Figure S12. SVD analysis of the pH series for (A) the Soret and (B) the charge-transfer regions of electronic absorption spectra for ferric T49V/K79G at 22 ± 2 °C. (C) Global fitting of the four most weighted V vectors from the SVD analyses yields pK_a values in Table S7. (D) Fractional populations of the components from SVD analyses using the pK_a values determined by the global fitting of the V vectors. Extracted spectra of the M state in the (E) Soret and (F) charge-transfer regions.

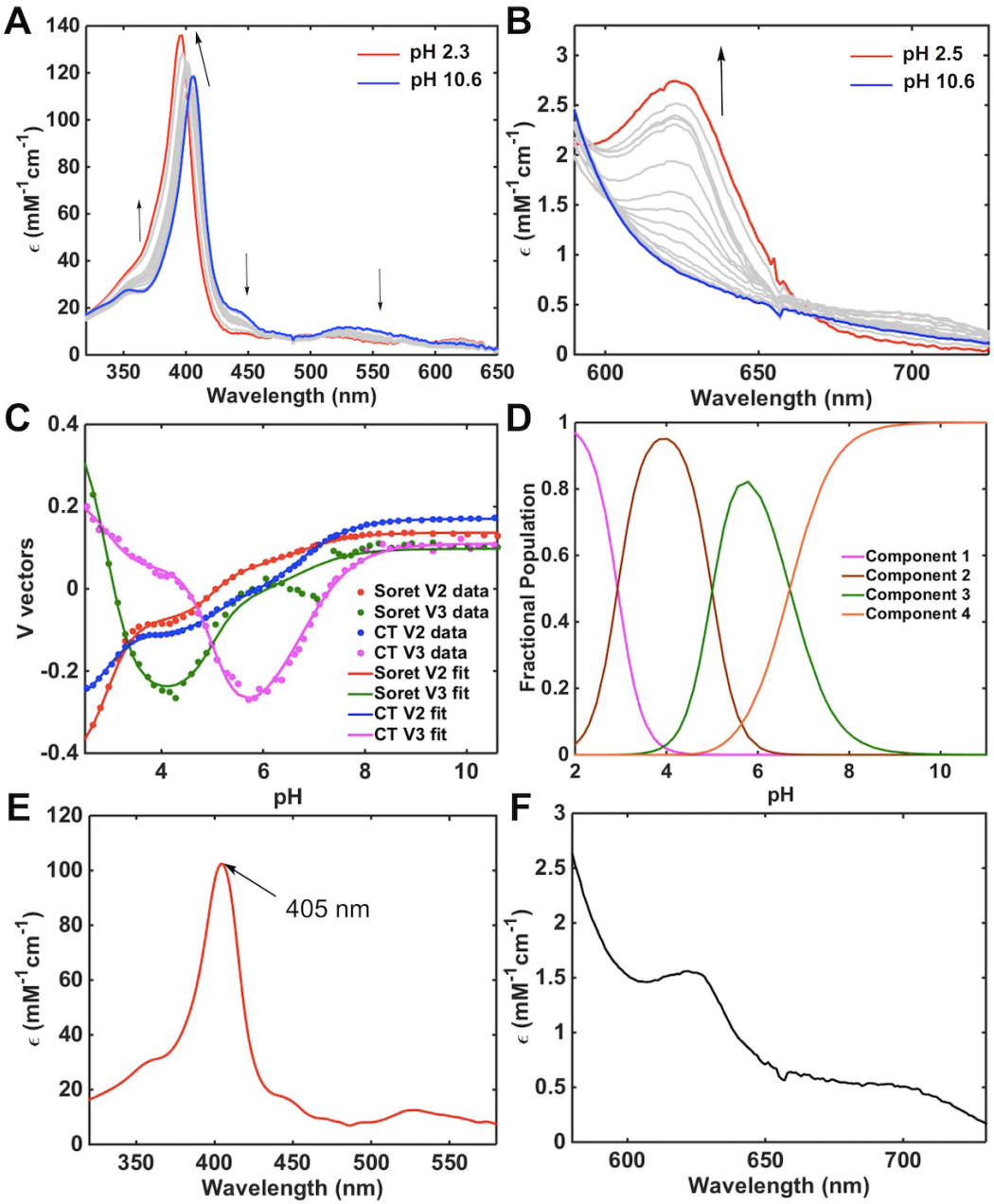

Figure S13. SVD analysis of the pH series for (A) the Soret and (B) the charge-transfer regions of electronic absorption spectra for ferric T78V/K79G at 22 ± 2 °C. (C) Global fitting of the four most weighted V vectors from the SVD analyses yields pK_a values in Table S7. (D) Fractional populations of the components from SVD analyses using the pK_a values determined by the global fitting of the V vectors. Extracted spectra of the M state in the (E) Soret and (F) charge-transfer regions.

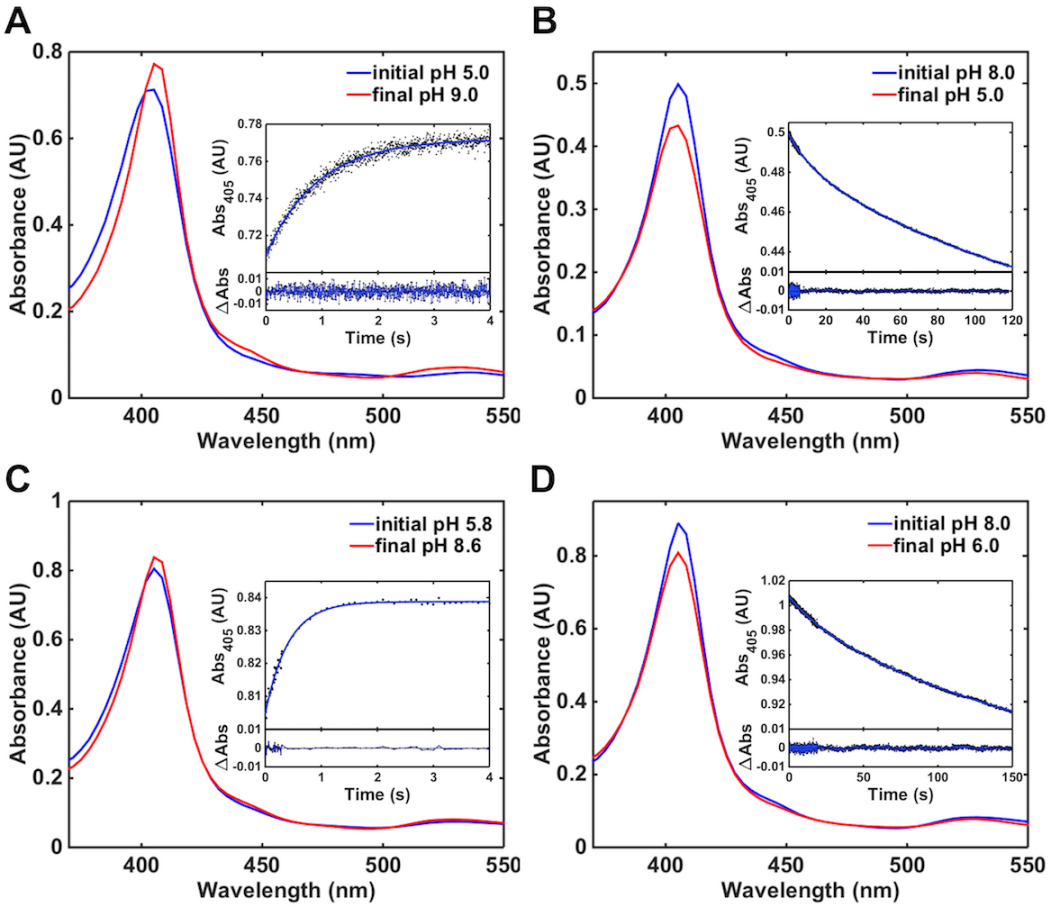

Figure S14. Representative plots of absorption spectra for ferric (A, B) T49V/K79G and (C, D) T78V/K79G at the initial (blue) and final (red) pH for upward (A, C) and downward (B, D) pH-jump experiments. The insets are changes in absorbance at 405 nm versus time and their fits to monoexponential rise (or decay) functions, together with residuals for the fits.

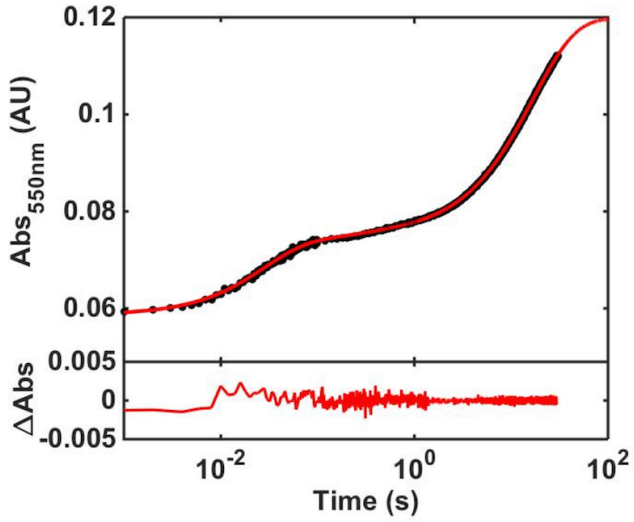

Figure S15. A representative progress curve showing absorbance changes at 550 nm for the bimolecular ET from a_6Ru^{2+} (0.21 mM) to ferric T49V/K79G (5 μM) at pH 7.0. The solid line (red) is a fit to a biexponential rise function. The residuals for the fit are shown at the bottom.

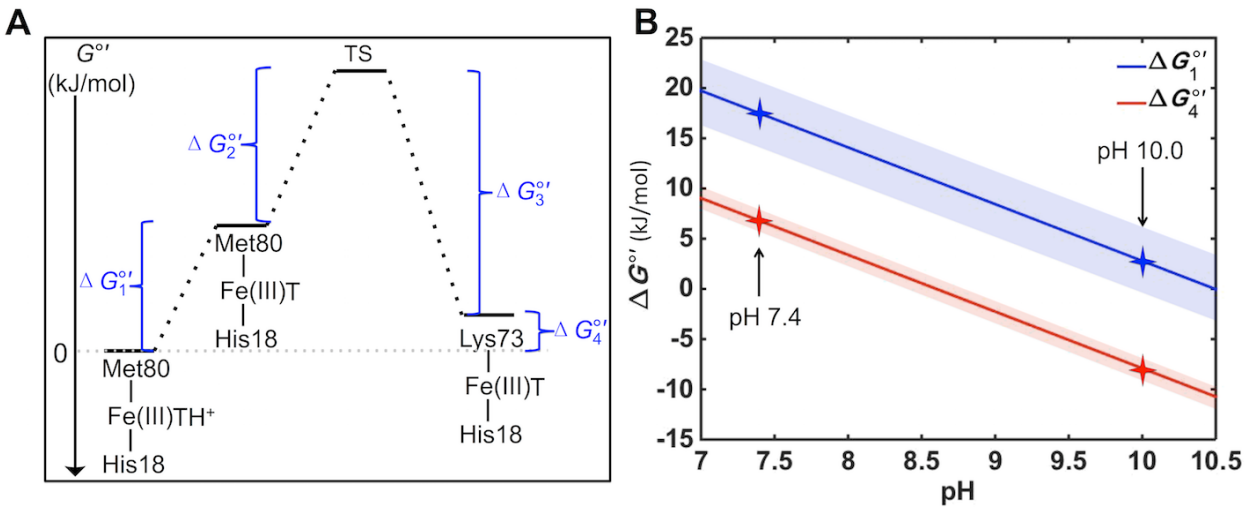

Figure S16. (A) Energy diagram for the alkaline transition in ferric K79G. Energy gaps between two states are labeled as $\Delta G_1^{\circ'}$ to $\Delta G_4^{\circ'}$. (B) Changes in $\Delta G_1^{\circ'}$ and $\Delta G_4^{\circ'}$ with pH are calculated using $\Delta G_1^{\circ'} = \mathrm{RT}\ln K_{\mathrm{C}}^{\mathrm{III}} - \mathrm{RT}\ln K_{\mathrm{eq}}^{\mathrm{III}}$ and $\Delta G_4^{\circ'} = -\mathrm{RT}\ln K_{\mathrm{eq}}^{\mathrm{III}}$. Error bars are displayed as shadows along each line (±3.7 kJ/mol for $\Delta G_1^{\circ'}$ and ±1.1 kJ/mol for $\Delta G_4^{\circ'}$). $\Delta G_2^{\circ'}$ and $\Delta G_3^{\circ'}$ are assumed not to change with pH.

Table S1. List of Reference Spectra of Cytochrome *c* Species Employed in SVD Analyses of pH Series

cyt *c* species	reference spectra
H_2O/H_2O unfolded	Determined by linear decomposition[a]
H_2O/His unfolded	M80A in 3 M GuHCl at pH 4.5
H_2O/His folded	M80A at pH 4.5
Met/His folded	WT* at pH 7.4
Lys/His folded	M80K*[2] at pH 7.4

[a]The spectrum of H_2O/H_2O unfolded species was determined by linear decomposition of the spectrum of M80A at pH 2. At pH 2, M80A is composed of 75% H_2O/H_2O unfolded and 25% H_2O/His unfolded species.[1]

Table S2. Structural Analysis of Snapshots from MD Simulations of Ferric Yeast *iso*-1 Cytochrome *c* Variants

Variant	SASA of heme group[a] (Å^2)	heme-pocket volume[a] (Å^3)	Wat166-Fe distance[b] (Å)	S(M80)-Fe distance[b] (Å)	N(H18)-Fe distance[b] (Å)	RMSD of C_α (Å)[c]
K79G	25.4±1.3	350±35	7.25	2.48	1.94	0
T49V/K79G	26.6±2.0	345±26	6.22	2.48	1.94	0.554
T78V/K79G	23.0±1.8	364±36	6.74	2.49	1.96	0.630

[a]Averaged values from the last thirty snapshots of the 0.13-ns MD simulation.

[b]For the averaged structural model of the last thirty snapshots.

[c]RMSD of the backbone C_α atoms for the averaged structural model relative to those for the averaged structural model of K79G.

Table S3. Structural Analysis of Snapshots from MD Simulations of Ferrous Yeast *iso*-1 Cytochrome *c* Variants

Variant	SASA of heme group[a] (Å^2)	heme-pocket volume[a] (Å^3)	Wat179-Fe distance[b] (Å)	S(M80)-Fe distance[b] (Å)	N(H18)-Fe distance[b] (Å)	RMSD of C_α (Å)[c]
K79G	23.0±1.7	338±32	6.98	2.49	1.94	0
T49V/K79G	24.9±1.3	373±24	6.86	2.49	1.94	0.664
T78V/K79G	23.6±1.3	346±26	6.67	2.49	1.91	0.625

[a]Averaged values from the last thirty snapshots of the 0.13-ns MD simulation.

[b]For the averaged structural model of the last thirty snapshots.

[c]RMSD of the backbone C_α atoms for the averaged structural model relative to those for the averaged structural model of K79G.

Table S4. Thermodynamic Parameters for the Unfolding Transitions of Ferric Yeast *iso*-1 Cytochrome *c* Variants at pH 4.5 Determined from Changes in Ellipticity at 222 nm

Variant	C_m^{III} (M)	m_D^{III} (kJ mol^{-1}M^{-1})	$\Delta G_u^{\circ\prime}(H_2O)^{III}$ (kJ mol^{-1})
K79G[3]	1.09±0.04	16.2±3.1	17.7±3.4
T49V/K79G	0.87±0.10	11.4±2.2	9.9±2.2
T78V/K79G	0.87±0.07	15.2±3.2	13.2±3.0

Table S5. Reduction Potentials[a] for Yeast *iso*-1 Cytochrome *c* Variants at Varying Scan Rates

Variant	pH	$E^{\circ'}$ (mV vs SHE)			
		0.02 V/s	0.1 V/s	20 V/s	
				Met-ligated	Lys-ligated
K79G	10.0	irreversible	239	258 ± 6	-145 ± 10
K79G	7.4	265	265	262 ± 3	not detected
T49V/K79G	7.4	187 ± 3	191 ± 3	197 ± 4	-141 ± 10
T78V/K79G	7.4	263	266	275 ± 3	-140 ± 4

[a]Reduction potentials (± 2 mV vs SHE, except where noted otherwise) from cyclic voltammetry at indicated scan rates. Buffers used were 0.1 M sodium phosphate at pH 7.4 and 20 mM CAPS with 0.1 M sodium acetate at pH 10.

Table S6. Reduction Potentials[a] for Yeast *iso*-1 Cytochrome *c* Variants at Varying pH

Variant	$E^{\circ'}$ (mV vs SHE)		
	pH 4.5	pH 6.0	pH 7.4
K79G	280	273	265
T49V/K79G	205	200	191± 3
T78V/K79G	258	278	266

[a]Reduction potentials (± 2 mV vs SHE, except where noted otherwise) as observed by cyclic voltammetry at 0.1 V/s. Buffers used were 0.1 M sodium phosphate at pH 7.4 and 6.0 and 0.1 M sodium acetate at pH 4.5.

Table S7. Results of Global Fitting of V Vectors from SVD Analyses of the pH Series of Electronic Absorption Spectra for Ferric Yeast *iso*-1 Cytochrome *c* Variants

T49V/K79G			T78V/K79G		
pK_a	*n*	Transition	pK_a	*n*	Transition
2.6±0.1	1.6±0.1	A1→A2	2.9±0.1	1.6±0.1	A1→A2
3.4±0.1	1.5±0.1	A2→M	5.0±0.1	1.5±0.1	A2→M
6.7±0.1	0.9±0.1	M→K	6.7±0.1	0.9±0.1	M→K

Table S8. Electron-transfer Parameters for Yeast *iso*-1 Cytochrome *c* Variants

Variant	$k_{ET,M}$ ($mM^{-1}s^{-1}$)	k_{ESE}[a] ($mM^{-1}s^{-1}$)
K79G	381.8±19.9[b,3]	12.1±1.2[b]
T49V/K79G	186.9±3.4	37.4±2.6
T78V/K79G	483.3±31.4	11.6±1.1

[a]These values were calculated using the Marcus cross relationship, $k_{ET,M} = (k_{11} \times k_{12} \times K_{12})^{1/2}$, where k_{11} is the k_{ESE} of the protein, k_{22} is the k_{ESE} of a_6Ru^{2+} (3×10^3 $M^{-1}s^{-1}$),[4] and K_{12} is the equilibrium constant for the cross-reaction. Values of K_{12} were determined by $K_{12} = \exp(nF\Delta E/RT)$, where ΔE is the difference of the reduction potentials of the Met-ligated protein variant and a_6Ru^{2+}.

[b]This calculated k_{ESE} value is within error the same as the experimentally determined value for this parameter.[3]

SI References

(1) Battistuzzi, G.; Bortolotti, C. A.; Bellei, M.; Di Rocco, G.; Salewski, J.; Hildebrandt, P.; Sola, M. Role of Met80 and Tyr67 in the low-pH conformational equilibria of cytochrome *c*. *Biochemistry* **2012**, *51*, 5967-5978.

(2) Amacher, J. F.; Zhong, F.; Lisi, G. P.; Zhu, M. Q.; Alden, S. L.; Hoke, K. R.; Madden, D. R.; Pletneva, E. V. A compact structure of cytochrome *c* trapped in a lysine-ligated state: loop refolding and functional implications of a conformational switch. *J. Am. Chem. Soc.* **2015**, *137*, 8435-8449.

(3) Deng, Y.; Zhong, F.; Alden, S. L.; Hoke, K. R.; Pletneva, E. V. The K79G mutation reshapes the heme crevice and alters redox properties of cytochrome *c*. *Biochemistry* **2018**, *57*, 5827-5840.

(4) Ewall, R. X.; Bennett, L. E. Reactivity characteristics of cytochrome *c*(III) adduced from its reduction by hexaammineruthenium(II) ion. *J. Am. Chem. Soc.* **1974**, *96*, 940-942.